

Cover Page



Universiteit Leiden



The handle <http://hdl.handle.net/1887/19771> holds various files of this Leiden University dissertation.

**Author:** Smeenk, Godelieve

**Title:** Chromatin remodelers in the DNA double strand break response

**Date:** 2012-09-11

# CHAPTER 2

## THE NURD CHROMATIN REMODELING COMPLEX REGULATES SIGNALING AND REPAIR OF DNA DAMAGE

Godelieve Smeenk<sup>1</sup>, Wouter W. Wiegant<sup>1</sup>, Hans Vrolijk<sup>2</sup>,  
Aldo P. Solari<sup>3</sup>, Albert Pastink<sup>1</sup> and Haico van Attikum<sup>1</sup>

<sup>1</sup> *Department of Toxicogenetics*, <sup>2</sup> *Department of Molecular Cell Biology and*  
<sup>3</sup> *Department of Medical Statistics, Leiden University Medical Center,*  
*Eindhovenweg 20, 2333ZC, Leiden, The Netherlands*

*Published in Journal of Cell Biology 2010 Sep 6; 190(5):741-9*

## SUMMARY

Cells respond to ionizing radiation (IR)-induced DNA double-strand breaks (DSBs) by orchestrating events that coordinate cell cycle progression and DNA repair. How cells signal and repair DSBs is not yet fully understood. A genome-wide RNAi screen in *C. elegans* identified *egr-1* as a factor that protects worm cells against IR. The human homologue of *egr-1*, MTA2, is a subunit of the NuRD chromatin remodeling complex. We show that knockdown of MTA2 and CHD4, the catalytic subunit (ATPase) of NuRD, leads to accumulation of spontaneous DNA damage and increased IR sensitivity. MTA2 and CHD4 accumulate in DSB-containing chromatin tracks generated by laser micro-irradiation. Directly at DSBs, CHD4 stimulates RNF8/RNF168-dependent formation of ubiquitin conjugates to facilitate the accrual of RNF168 and BRCA1. Finally, we show that CHD4 promotes DSB repair and checkpoint activation in response to IR. Thus, the NuRD chromatin remodeling complex is a novel regulator of DNA damage responses that orchestrates proper signaling and repair of DSBs.

## INTRODUCTION

The efficient and accurate repair of chromosomal double-strand breaks (DSBs), which may arise from exposure to agents such as ionizing radiation (IR), is critical in maintaining genome stability and preventing cell death and carcinogenesis. To avoid deleterious effects of DSBs eukaryotic cells activate signaling cascades, called checkpoints, which coordinate rapid detection of DNA breaks with a temporal arrest in cell cycle progression and activation of DNA repair mechanisms (Khanna and Jackson, 2001; Hoeijmakers, 2001).

The cellular response to DSBs is predominantly coordinated by the phosphatidylinositol 3-kinase-like kinases (PIKKs) ATM and ATR. ATM phosphorylates histone H2AX ( $\gamma$ H2AX) in DSB-flanking chromatin to create an environment that allows for the spatio-temporal redistribution and accumulation of checkpoint and DNA repair factors at DNA breaks (van Attikum and Gasser, 2009). Among the first proteins to arrive at DSBs is MDC1, which directly binds to  $\gamma$ H2AX (Stucki et al., 2005). This allows for the recruitment of the E2 ubiquitin conjugase UBC13 and the E3 ubiquitin ligase RNF8, the latter of which binds to MDC1 (Huen et al., 2007; Kolas et al., 2007; Mailand et al., 2007). RNF8/UBC13 promote the ubiquitylation of histones H2A/H2AX, leading to the recruitment of another E3 ubiquitin ligase, RNF168, which associates with RNF8-ubiquitylated histones via its ubiquitin-interacting motifs (UIMs) (Doil et al., 2009; Huen et al., 2007; Kolas et al., 2007; Mailand et al., 2007; Stewart et al., 2009). RNF168 cooperates with UBC13 to amplify RNF8-mediated histone ubiquitylation to a threshold required for the accumulation of checkpoint and repair proteins, including BRCA1, 53BP1, RAD18 and PTIP, in the DSB-flanking chromatin compartment (Huang et al., 2009; Gong et al., 2009; Doil et al., 2009; Stewart et al., 2009; Wang and Elledge, 2007). In addition to these ATM-driven events, DSB ends undergo extensive resection, leading to the formation of RPA-coated single-stranded DNA and subsequent assembly and activation of ATR (Zou and Elledge, 2003; Jazayeri et al., 2006; Dubrana et al., 2007). Finally, ATM and ATR amplify the signals generated at DSBs by phosphorylating a number of regulatory proteins, including SMC1, CHK1, CHK2, p53 and p21, that coordinate cell cycle progression or induce apoptosis (Khanna and Jackson, 2001; Shiloh, 2003).

The crosstalk between histone modifications (e.g. phosphorylation and ubiquitylation) in DSB-flanking chromatin controls ATM/ATR-dependent signaling and repair of DSBs, yet it is unclear how this is achieved (van Attikum and Gasser, 2009). One possible mechanism may be ATP-dependent chromatin remodeling carried out by ATPases of the SNF2 superfamily (Clapier and Cairns, 2009). We and others have previously demonstrated in budding yeast that several chromatin remodeling complexes (INO80, SWR1, SWI/SNF and RSC) are recruited to DSBs, where they change chromatin structure in distinct ways to regulate cell cycle progression and/or DSB repair (Morrison et al., 2004; Papamichos-Chronakis et al., 2006; Tsukuda et al., 2005; van Attikum et al., 2007; van Attikum et al., 2004; Chai et al., 2005; Liang et al., 2007; Shim et al., 2007; Shim et al., 2005). In contrast to budding yeast, in

human cells the role of chromatin remodeling during the cellular response to DSBs is just beginning to emerge. The TIP60 and SWI/SNF chromatin remodeling complexes, for example, have been implicated in DNA repair by promoting histone acetylation and H2AX phosphorylation at DSBs, respectively (Ikura et al., 2007; Murr et al., 2006; Park et al., 2006), while ALC1 has recently been shown to assist in PARP-dependent chromatin remodeling at sites of DNA damage (Ahel et al., 2009; Gottschalk et al., 2009). It is unclear, however, how the interplay between chromatin remodeling and histone modifications at DSBs coordinates cell cycle progression and DNA repair.

Here we identify the Nucleosome Remodeling and histone Deacetylation (NuRD) complex as a novel regulator of the DSB response in human cells. NuRD prevents the accumulation of spontaneous DNA damage and regulates apoptotic responses through p53 and p21. Moreover, NuRD is rapidly recruited to DSBs, where it promotes RNF8/RNF168-mediated histone ubiquitylation and the ubiquitin-dependent accumulation of RNF168 and BRCA1. Consequently, loss of NuRD components causes defects in DNA repair and checkpoint activation, rendering cells hypersensitive to IR. Thus, the NuRD chromatin remodeling complex is a novel DNA damage response factor that helps to preserve genome stability by regulating signaling and repair of DNA damage.

## RESULTS AND DISCUSSION

### CHD4 preserves genome stability and prevents apoptosis

We previously performed a genome-wide RNAi screen in the nematode *Caenorhabditis elegans* and identified 45 genes that protect worms against IR (van Haften et al., 2006). Among these genes were well-known DNA damage response (DDR) factors, as well as several novel genes, including *egr-1/lin-40*. *egr-1* encodes for a protein that is homologous to metastasis-associated protein 2 (MTA2), which is a component of the NuRD complex (Xue et al., 1998; Zhang et al., 1999). Biochemical studies indicated that MTA2 modulates the histone deacetylation activity of NuRD (Zhang et al., 1999). The chromatin remodeling activity of this complex resides within another subunit, chromodomain helicase DNA-binding protein 4 (CHD4), which was first identified as a dermatomyositis-specific autoantigen (Seelig et al., 1995). CHD4 is a member of the SNF2 family of ATPases and possesses intrinsic ATP-dependent nucleosome remodeling activity (Wang and Zhang, 2001). It is thought that NuRD represses transcription by regulating chromatin structure (Denslow and Wade, 2007). Moreover, a recent report showed that loss of several NuRD components results in chromatin defects that are associated with DNA damage accumulation and ageing (Pegoraro et al., 2009). However, whether NuRD preserves genome stability and regulates the DDR remained unclear.

To investigate this we transfected U2OS cells with siRNAs against luciferase or CHD4 and counted cells 2, 3 and 4 days after siRNA treatment. CHD4 knockdown cells proliferated much slower than control cells (Fig. 1, A and B). Flow cytometric analysis of these cells did not show any significant changes in cell cycle distribution.

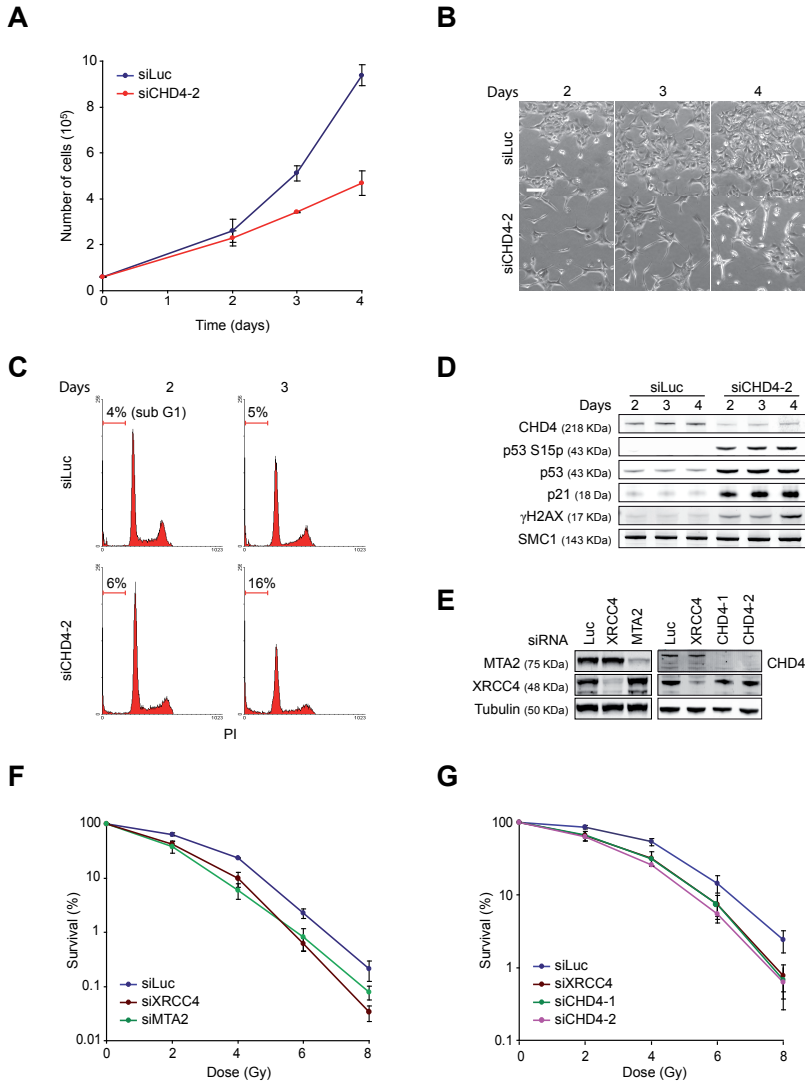


**Figure 1. MTA2 or CHD4 depletion renders cells sensitive to IR.** (A) Depletion of CHD4 reduces cell proliferation. U2OS cells were transfected with the indicated siRNAs. Cells were counted 0, 2, 3 and 4 days after siRNA transfection. Graphs represent the mean  $\pm$  s.e.m. of 3 independent experiments. (B) Pictures from representative areas of the cell dishes from A. Scale bar, 200  $\mu$ m. (C) FACS analysis of cells from A. (D) CHD4 depletion leads to enhanced levels of phosphorylated p53 (S15p), p53, p21, and  $\gamma$ H2AX. Protein levels were monitored by western blot analysis using whole cell extracts (WCE) from cells in A. SMC1 is a loading control. (E) CHD4, MTA2 and XRCC4 levels were monitored by western blot analysis using WCE of cells in F and G. Tubulin is a loading control. (F) MTA2 depletion renders cells hypersensitive to IR. VH10-SV40 cells were transfected with the indicated siRNAs. Graphs represent the mean  $\pm$  s.e.m. of 3 independent experiments. (G) CHD4 depletion renders cells hypersensitive to IR. As in F, except that siRNAs against CHD4 were used.

However, morphological changes and marked sub-G1 peaks, indicative of apoptosis, were observed 2-4 days after siRNA transfection (Fig. 1, B and C). Consistently, the levels of p53, phosphorylated p53 (S15p), and the p53-effector p21, which coordinate cell cycle progression and apoptosis, were significantly increased in the absence of CHD4 (Fig. 1 D), in agreement with an earlier report implicating a role for NuRD in apoptosis and p53/p21 regulation (Luo et al., 2000). We investigated whether apoptosis induced by loss of CHD4 might be related to the spontaneous occurrence of DNA lesions. Indeed, CHD4 knockdown cells showed increased levels of  $\gamma$ H2AX as early as 2 days after siRNA transfection (Fig. 1 D), corroborating findings from a recent study (Pegoraro et al., 2009). Hence, CHD4 depletion leads to the accumulation of spontaneous DNA damage and activation of the apoptotic p53/p21 program. We infer that NuRD prevents genome instability and apoptosis.

### **CHD4 and MTA2 protect cells against the clastogenic effects of IR**

EGR-1 (MTA2) protects worm cells against IR (van Haafden et al., 2006). To examine whether MTA2 also protects human cells against IR, we tested whether its depletion affects clonogenic survival of VH10-SV40 cells. Loss of MTA2 led to an increase in IR sensitivity that was comparable with that observed in XRCC4 knockdown cells, which are impaired in DSB repair by non-homologous end-joining (Grawunder et al., 1998) (Fig. 1, E and F). In addition, we found that CHD4-depleted cells show increased IR sensitivity (Fig. 1, E and G). Thus, both MTA2 and CHD4 protect cells against the effects of IR, implicating a role for NuRD in the cellular response to DSBs. Furthermore, MTA2 protects both worm and human cells against IR, which may suggest that its putative role in the DDR is conserved.

### **CHD4 controls the p53/p21-axis of the IR-induced DDR**

To investigate the role of NuRD in the DDR, we examined whether CHD4 depletion affects ATM/ATR-dependent phosphorylation of DDR components in response to IR. Knockdown of CHD4 did not impair IR-induced ATM activation or  $\gamma$ H2AX formation, but led to increased levels of  $\gamma$ H2AX in unirradiated cells, corroborating our previous result (Figs. 1 D, 2 A and S1). We then investigated whether CHD4 mediates ATM/ATR-dependent activation of downstream effectors SMC1 (S966p), CHK1 (S317p), CHK2 (S19p), p53 (S15p) and p21, of the DDR. We repeatedly observed a small increase in the phosphorylation of SMC1 and CHK1, but not of CHK2 within the first 30 minutes after IR exposure (data not shown). In addition, we observed a small accumulation of CHD4-depleted cells in mid-S-phase, suggesting that this "aberration" in the phosphorylation status of SMC1 and CHK1, which are regulators of IR-induced intra-S-phase checkpoints, has a weak effect on cell cycle progression (Fig. 2, B and C). Loss of CHD4, however, enhanced the levels of total p53 and phosphorylated p53 after exposure to IR. This was accompanied by an increase in p21 levels 24 h after IR treatment (Fig. 2 A). p53 and p21 play a prominent role in the G1 checkpoint response (Khanna and Jackson, 2001; Shiloh, 2003). Accordingly, we

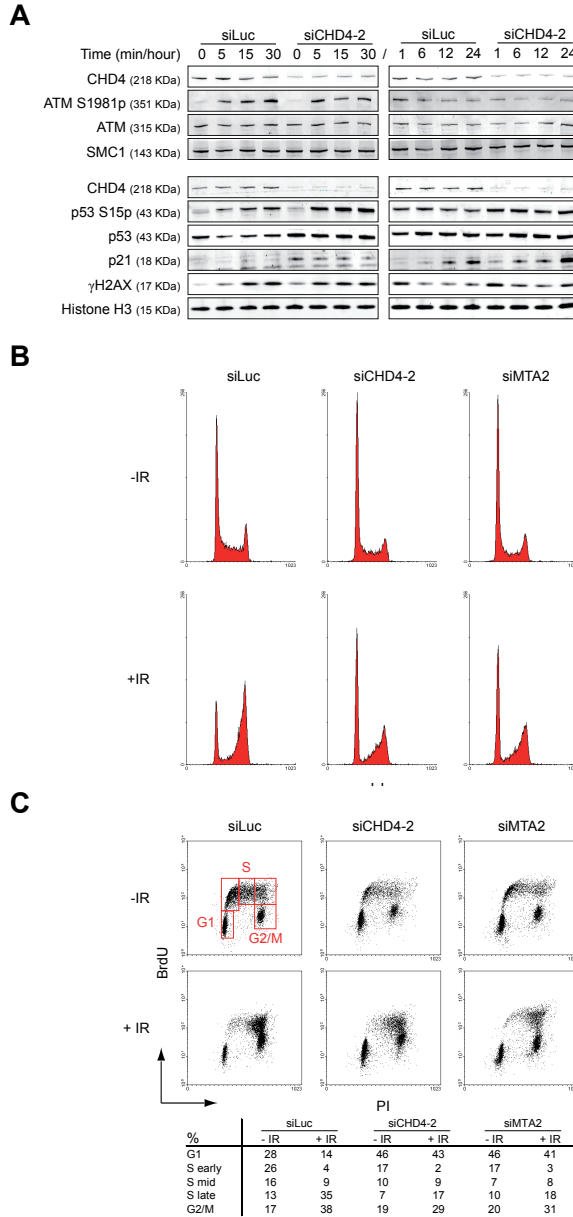


**Figure 2. CHD4 controls IR-induced p53/p21 responses.** (A) CHD4 depletion increases IR-induced p53 phosphorylation (S15p), p53 and p21 levels. U2OS cells were transfected with the indicated siRNAs and exposed to 6 Gy of IR. WCE were prepared at the indicated time points and  $\gamma$ H2AX, ATM S1981p, ATM, CHD4, p53 S15p, p53 and p21 levels were monitored by western blot analysis. Histone H3 and SMC1 were loading controls. (B) CHD4- and MTA2-depleted cells accumulate in G1-phase and remain in G1-arrest after exposure to IR. U2OS cells were transfected with the indicated siRNAs for 72 h, exposed to 6 Gy of IR and 12 h later subjected to FACS. (C) As in B, except that cells were stained with BrdU.

detected an arrest of CHD4-depleted cells in G1-phase that was maintained after IR exposure (Fig. 2, B and C). This suggests that CHD4 controls p53/p21-dependent G1 checkpoint responses induced by IR.

### NuRD rapidly accumulates within DSB-flanking chromatin

The DSB response is characterized by the accumulation of checkpoint and DNA repair proteins in DSB-flanking chromatin. To investigate whether NuRD plays a direct role in the DDR we examined recruitment of several of its subunits (CHD4, MTA2 and MBD3) to sites of DNA damage. We found that GFP-tagged CHD4, MTA2 and MBD3 accumulate in micro-laser generated DSB-tracks and span the entire chromatin region that was marked by  $\gamma$ H2AX (Figs. 3 A and S2 A), a characteristic shared with other known DSB-associated factors (Bekker-Jensen et al., 2006). Furthermore, they were rapidly recruited to DSB-tracks and accumulated with similar kinetics. Accumulation became detectable within 30 seconds, reaching half-maximum at 40 seconds and steady-state levels at 3 minutes, respectively (Fig. 3, B and C; Fig. S2, B and C).

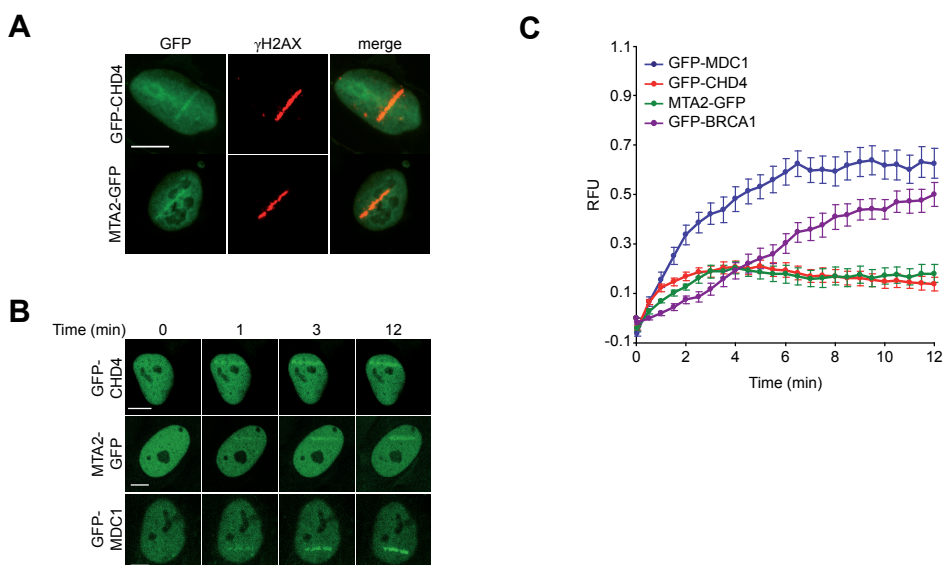


**Figure 3. CHD4 and MTA2 rapidly accumulate at sites of DNA damage.** (A) CHD4 and MTA2 accumulate in DSB-containing regions marked by  $\gamma$ H2AX. U2OS cells transiently expressing GFP-CHD4 or MTA2-GFP were subjected to laser micro-irradiation. After 15 min cells were immunostained for  $\gamma$ H2AX. (B) GFP-CHD4 and MTA2-GFP, like GFP-MDC1, rapidly accumulate in DSB-containing regions. U2OS cells transiently expressing GFP-CHD4, MTA2-GFP or GFP-MDC1 were micro-irradiated as in A and subjected to real-time recording of protein assembly at the damaged area. (C) Quantitative representation of the results in B. U2OS cells transiently expressing GFP-BRCA1 were included. Relative Fluorescence Units (RFU) are plotted on a time scale. Graphs represent the mean  $\pm$  s.e.m. of at least 10 individual cells from at least 2 independent experiments. Scale bars, 10  $\mu$ m.

Mailand and colleagues recently defined two distinct kinetic groups of proteins that arrive either “early” (e.g. MDC1 and RNF8) or “late” (e.g. BRCA1 and 53BP1) at the DSB-track (Mailand et al., 2007). We demonstrated that GFP-CHD4, MTA2-GFP and GFP-MBD3 arrive at the DSB-track as early as GFP-MDC1 (Figs. 3 C and S2 C). Interestingly, they reached their steady state levels of accumulation significantly faster than MDC1 and BRCA1. This may suggest that these NuRD subunits do not occupy DSB-containing chromatin to the same level as these core components of the DSB response (Figs. 3 C and S2 C). We conclude that NuRD is among the factors that assemble early in DSB-flanking chromatin.

### **CHD4 regulates DSB-associated ubiquitylation to orchestrate the accumulation of RNF168 and BRCA1**

To examine whether NuRD modulates early events of the DSB response, we analyzed IRIF (ionizing radiation-induced foci) formation of  $\gamma$ H2AX, since this histone mark acts as a docking site for MDC1/RNF8 at DSBs (Stucki et al., 2005). CHD4 knockdown, however, did not affect  $\gamma$ H2AX IRIF formation (Fig. 4 A), which corroborates our western blot analysis showing proper IR-induced  $\gamma$ H2AX formation in the absence of CHD4 (Figs. 2 A and S1). Accordingly, MDC1 and RNF8 IRIF formation were also not affected by the loss of CHD4 (Fig. 4, A and B).

In contrast, the accumulation of conjugated ubiquitin into IRIF was impaired in CHD4-depleted cells (~2-fold; Fig. 4 C and D). Consistently, we observed a distinct reduction in IRIF formation of RNF168 and BRCA1, which have been shown to bind to DSB-associated ubiquitin moieties (Fig. 4, C and D), the formation of which may require CHD4. Indeed, we found that CHD4 knockdown, like RNF8 knockdown, significantly decreased the level of  $\gamma$ H2AX mono- and di-ubiquitylation after IR (Fig. S3, A and B) (Huen et al., 2007). Because the total levels of endogenous MDC1, RNF8, RNF168 and BRCA1 were not affected by CHD4 depletion, we conclude that the observed defects in IRIF formation resulted from a reduction in RNF8/RNF168-dependent ubiquitylation and subsequent RNF168 and BRCA1 accumulation at DSBs (Fig. S1). Moreover, expression of a dominant negative, ATPase-dead form of CHD4 (GFP-CHD4 K757R) reduced RNF168 IRIF formation (Fig. S3, C and D), suggesting that ATP-dependent chromatin remodeling driven by the CHD4 ATPase triggers this process.

Thus, NuRD-mediated chromatin remodeling facilitates RNF8/RNF168-dependent histone ubiquitylation to orchestrate the accumulation of RNF168 and BRCA1. NuRD may change nucleosome structures such that the otherwise inaccessible RNF8/RNF168 H2A-type histone targets become amenable for ubiquitylation.

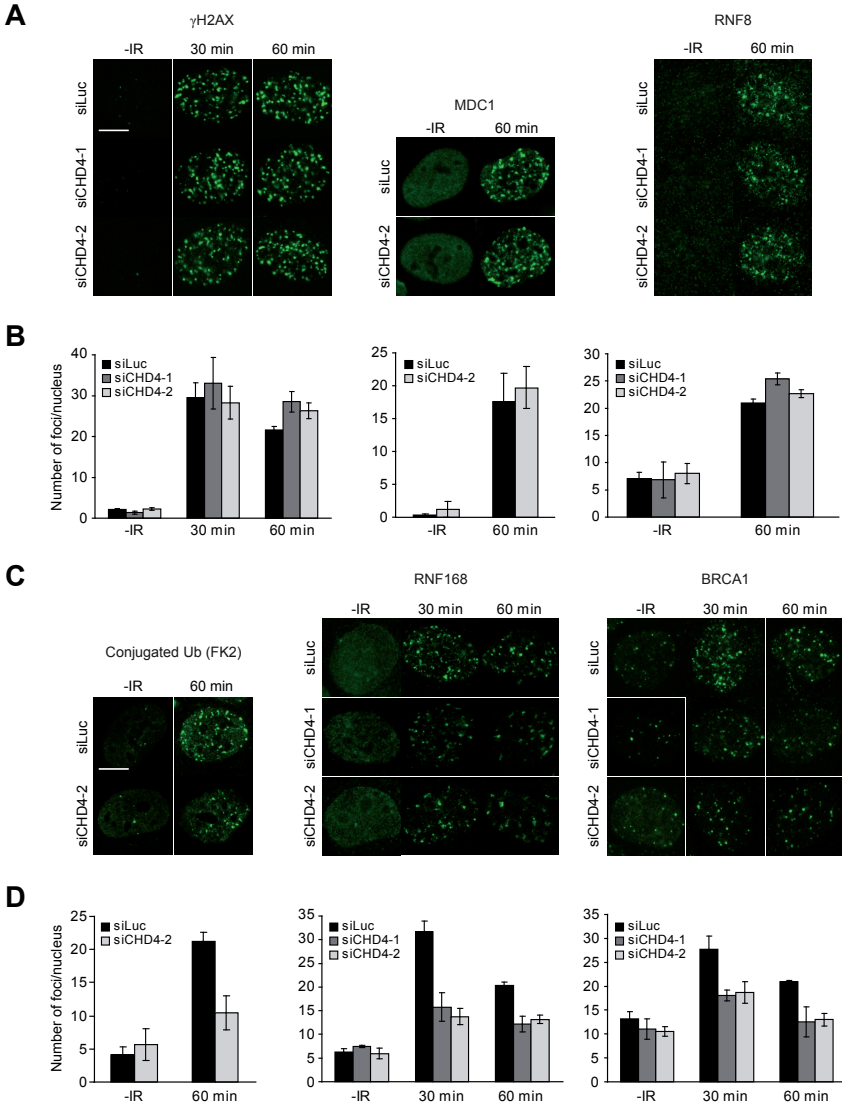


**Figure 4. CHD4 promotes histone ubiquitylation at DSBs to orchestrate the accumulation of RNF168 and BRCA1.** (A) CHD4 depletion does not alter  $\gamma$ H2AX, MDC1 and RNF8 IRIF formation. Cells were transfected with the indicated siRNAs, exposed to 1 Gy of IR and 30 and/or 60 min later immunostained for  $\gamma$ H2AX, MDC1 or RNF8. Scale bar, 10  $\mu$ m. (B) Quantitative analysis of  $\gamma$ H2AX, MDC1 and RNF8 IRIF formation. The average number of foci/nucleus  $\pm$  s.e.m. is presented. More than 150 nuclei from cells in A were scored per time point in at least 2 independent experiments. (C) CHD4 depletion impairs ubiquitin, RNF168 and BRCA1 IRIF formation. As in A, except that cells were immunostained for conjugated ubiquitin (FK2), RNF168, and BRCA1. Scale bar, 10  $\mu$ m. (D) Quantitative analysis of ubiquitin, RNF168 and BRCA1 IRIF formation (as in B).

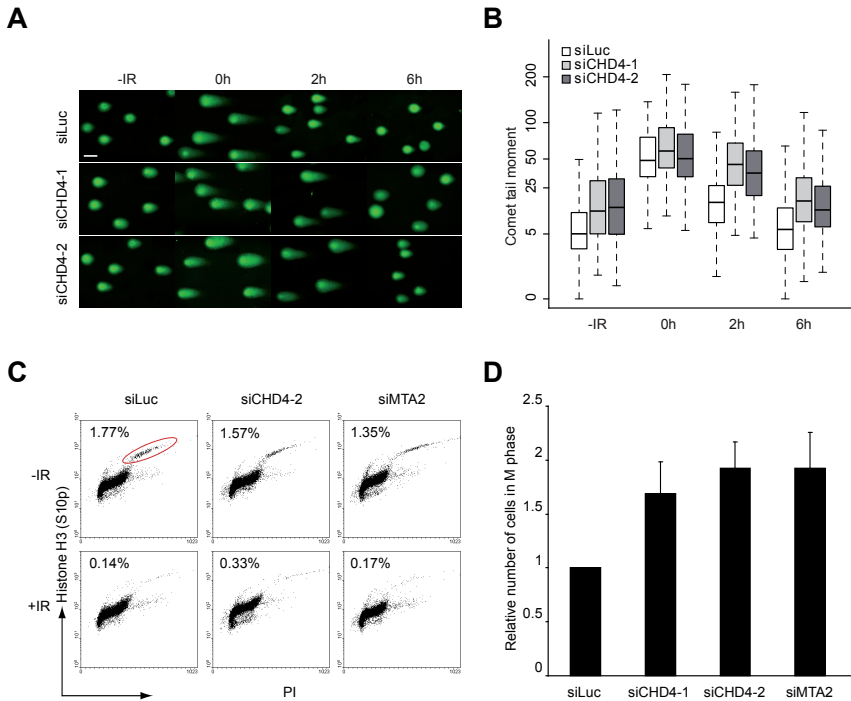
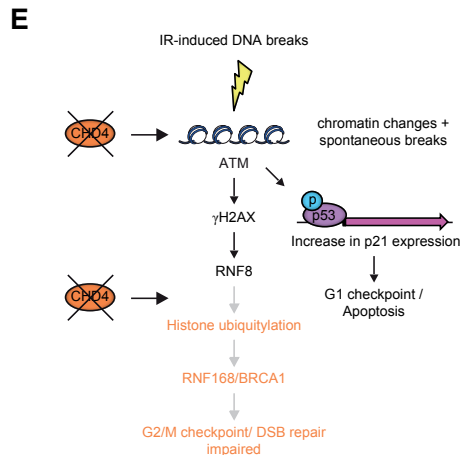


**Figure 5. CHD4 promotes DSB repair and IR-induced activation of the G2/M checkpoint.**

(A) CHD4 depletion impairs DSB repair. VH10-TERT cells were transfected with the indicated siRNAs for 72 h, exposed to 20 Gy of IR and subjected to neutral comet analysis at the indicated time points. Representative images are shown. Scale bar, 30  $\mu$ m. (B) Quantification of tail moments using cells from A. Tail moments for each condition were calculated on a minimum of 300 cells for each data point. Results of 4 independent experiments are shown as a box-and-whisker plot. The ordinate is a cube root scale. Data were statistically analysed using a two-way ANOVA, which revealed a significant delay in DSB repair for CHD4-depleted cells at 2h after IR ( $p < 0.0001$ ). (C) CHD4 or MTA2 depletion impairs IR-induced G2/M checkpoint activation. U2OS cells were transfected with the indicated siRNAs, exposed to 3 Gy of IR and 1 h later immunostained for phosphorylated histone H3 (S10p). Mitotic indexes were determined by FACS. A representative experiment is shown. (D) Graphical representation of relative mitotic index values. The ratio of index values from irradiated and unirradiated cells was calculated and normalized to that for control cells, which was set to 1. The mean  $\pm$  s.e.m. of 4 experiments is shown. (E) Model for the role of CHD4 in the maintenance of genome stability. See the last paragraph of the results and discussion section for details.



## CHD4 and MTA2 promote DSB repair and G2/M checkpoint activation

RNF168 and BRCA1 promote DSB repair and G2/M checkpoint activation in response to IR (Xu et al., 2001; Xie et al., 2007; Moynahan et al., 1999; Stewart et al., 2009; Doil et al., 2009). Given that CHD4 facilitates the accumulation of these proteins in DSB-flanking chromatin, we examined its role in DSB repair and G2/M checkpoint activation.

Neutral comet assays were performed to determine the effect of CHD4 knockdown on the rejoining of IR-induced DSBs in VH10-TERT cells. As shown in figure 5 (panels A and B), we detected a pronounced increase in the level of DSBs in unirradiated CHD4-depleted cells. This is consistent with the elevated levels of total  $\gamma$ H2AX observed earlier (Fig. 1D and 2A), and implies that spontaneous DSBs accumulate in the absence of CHD4 (Fig. 1D). Importantly, the level of IR-induced DSBs remained higher at 2 hours in CHD4 knockdown cells, but returned to basal levels at 6 hours. This suggests that CHD4 promotes proper DSB repair (Fig. 5, A and B).

Next, we tested the effect of CHD4 and MTA2 depletion on IR-induced G2/M checkpoint activation. We found that CHD4- and MTA2-depleted cells, like those depleted of BRCA1 or RNF8 (Xu et al., 2001; Huen et al., 2007; Kolas et al., 2007), failed to fully activate the G2/M checkpoint and continued to enter mitosis (Fig. 5, C and D), indicating that CHD4 and MTA2 facilitate full-scale activation of the G2/M checkpoint.

In conclusion, we report on the identification and characterization of the NuRD chromatin remodeling complex as a novel factor involved in genome surveillance. The lack of CHD4 consistently led to increased levels of spontaneous DNA damage, a phenotype that was associated with the activation of p53 and p21 responses, reduced cell proliferation and apoptosis. We propose that loss of chromatin remodeling by NuRD induces genome-wide chromatin alterations, which render chromatin more susceptible to spontaneous DNA breaks (Fig. 5 E). Support for such a scenario comes from a recent report which demonstrated that loss of several NuRD components during premature and normal ageing was associated with changes in higher-order chromatin structure, including loss of heterochromatic regions, and an accumulation of spontaneous DNA damage (Pegoraro et al., 2009).

We also provide evidence for a direct role of NuRD in the DSB response as several NuRD components (CHD4, MTA2 and MBD3) assemble at DSBs. Loss of CHD4 uncoupled the DSB response at the level of RNF8/RNF168-mediated histone ubiquitylation, leading to defects in the assembly of RNF168 and BRCA1. This most likely attenuated DSB repair and activation of the G2/M checkpoint and contributed to the IR sensitivity observed in CHD4- or MTA2-depleted cells (Fig. 5 E). Thus, NuRD is a novel factor that preserves genome stability by modulating chromatin structure (1) genome-wide to prevent spontaneous DNA damage and (2) at DNA breaks to orchestrate a proper DSB response (see also accompanying paper by Larsen et al.). Our work provides a framework for future studies that will gain more insight in the crosstalk between chromatin remodeling and mechanisms involved in genome maintenance.

## MATERIALS AND METHODS

### Cell culture and chemicals

Human U2OS, VH10-SV40- and VH10-TERT-immortalized fibroblasts were grown in DMEM (Gibco) containing 10% FCS (Bodinco BV). siRNA and plasmid transfections were performed using HiPerfect (Qiagen) and JetPEI (Polyplus Transfection), respectively, according to the manufacturer's instructions. The following siRNA sequences were used: 5'-CGUACGCGGAAUACUUCGA-3' (Luciferase), 5'-CCAAGGACCUGAAUGAUGA-3' (CHD4-1, Dharmacon), 5'-CAAAGGUGCUGCUGAUGUA-3' (CHD4-2, Dharmacon), 5'-CAAAGUCUCUCUCCUUACAUU-3' (MTA2, Dharmacon), 5'-GAGGGCC-AAUGGACAAUUA-3' (RNF8, Dharmacon), 5'-AUAUGUUGGUGAACUGAGA-3' (XRCC4) (Sartori et al., 2007). Cells were examined 48 h after siRNA transfection unless otherwise stated. The cDNAs for human CHD4 (Open Biosystems) and MTA2 (Imagenes) were cloned into pEGFP-C1 and pEGFP-N1, respectively (Clontech). The point mutation K757A was introduced into pEGFP-C1-CHD4 by site-directed mutagenesis. The pGFP-MBD3, GFP-BRCA1 and GFP-MDC1 constructs were gifts from Adrian Bird, Ody Sibon and Jiri Lukas, respectively.

### Generation of DSBs

DSBs were induced by IR, which was delivered by the YXlon X-ray generator (YXlon International, 200KV, 4 mA, dose rate 1.1 Gy/min).

### Cell survival assay

VH10-SV40 cells were transfected for 48 h, trypsinized, seeded at low density and exposed to IR. 7 days later cells were washed with 0.9% NaCl and stained with methylene blue. Colonies of more than 20 cells were scored.

### Microscopy and laser micro-irradiation

Brightfield pictures were taken with an EVOS fl fluorescence microscope (AMG, Westover Scientific) using the 4x Ph objective. Laser micro-irradiation was carried out on a Leica TCS SP5/AOBS confocal microscope equipped with an environmental chamber set to 37°C and 5% CO<sub>2</sub>. Cells were grown on glass bottom dishes (MatTek) in colorless medium containing 10% FCS (Gibco) and Hoechst 33342 was added to the medium at a concentration of 0.5 µg/ml prior to laser irradiation. DSB-containing tracks (0.5 x 10µm) were generated with a Diode laser ( $\lambda= 405\text{nm}$ , 30% laser power, 0.75 sec irradiation time, 2220 µW) using the UV-transmitting HCX PL APO 63X/1.4 NA oil immersion objective. Confocal images were recorded before and after laser irradiation at 20 or 30 sec time intervals over a period of 5 or 12 min and analyzed using LAS-AF software. Fluorescence intensities were corrected for background and normalized to pre-bleach values to determine recruitment kinetics.

## Antibodies

IRIF and western blot analysis were performed using antibodies to  $\gamma$ H2AX (Millipore),  $\alpha$ -Tubulin (Sigma), ATM (GeneTex), ubiquitin (FK2, Enzo Life Sciences), BRCA1 (Calbiochem), histone H3, ATM S1981p, MDC1, MTA2, CHD4 and RNF8 (Abcam), p53 and p21 (Santa Cruz), p53 S15p (Cell Signaling), and SMC1 (Bethyl Laboratories). The antibodies to RNF168 and XRCC4 were gifts from Dan Durocher and Mauro Modesti, respectively.

## IRIF analysis

Cells were grown on glass coverslips and treated as indicated in the figure legends. Subsequently, cells were washed with PBS, fixed with 2% formaldehyde and 0.25% Triton X-100 in PBS and incubated with appropriate primary and secondary antibodies (AlexaFluor 488, Invitrogen or goat anti-rabbit IgG conjugated to Cy3, Jackson Immunoresearch) and DAPI. An additional extraction with 0.25% Triton in CSK buffer (10 mM Hepes, 2 M KOH, 300 mM Sucrose, 100 mM NaCl, 3 mM  $MgCl_2$ ) was performed prior to fixation and incubation with primary antibodies against RNF168 and BRCA1. Images were recorded with a Zeiss Axioplan microscope using a 63x/1.25 NA oil objective and an Axiocam mRm camera, and analyzed using home-made Stacks software. Nuclei were detected and selected by global thresholding of DAPI images. Then contour tracing was performed after which pixels were labeled with a unique object index that determines to which nucleus the pixels belong. The actual detection of the foci was carried out on Alexa488 or Cy3 images. First a top-hat transformation was performed to reduce the influence of variation in background staining within nuclei. On the resulting image a watershed algorithm was carried out to determine the location of foci within the image by providing a unique spot index to the pixels of each focus. By combining foci indices with object indices obtained from the DAPI image, foci could be assigned to the nuclei in which they were detected, allowing calculation of the number of foci per nucleus.

## Chromatin fractionation and western blotting

Chromatin-enriched extracts were prepared and used for immunoprecipitation as described previously (Huen et al., 2007). Whole cell extracts (WCE) were prepared by cell lysis in Laemmli buffer. Proteins were separated in Bis-Tris-HCl-buffered acrylamide gels (Invitrogen) and blotted onto either PVDF (Millipore) or nitrocellulose (Amersham Biosciences). Membranes were incubated with primary antibody as indicated in the figure legends, followed by incubation with secondary antibody (Odyssey IRDye<sup>®</sup> Li-Cor Biosciences). The Odyssey imager (Li-Cor Biosciences) equipped with Li-Cor Odyssey 3.0 software was used to scan the membranes and analyze the fluorescence signals.

## Fluorescence-Activated Cell Sorting (FACS)

For G2/M checkpoint analysis cells were fixed in 70% ethanol, stained with rabbit antibody to histone H3 S10p (Millipore), followed by incubation with conjugated anti-rabbit IgG (AlexaFluor 488). For cell cycle analysis cells were pulse-labeled with 10  $\mu$ M BrdU for 1 h, fixed in 70% ethanol, denatured in 2 M HCl, stained with mouse antibody to BrdU, followed by incubation with conjugated anti-mouse IgG (AlexaFluor 488) and DNA staining with 0.1 mg/ml Propidium Iodide. Cell sorting was performed on a BD LSRII flow cytometer (BD Bioscience) using FACSDiva software version 5.0.3. Quantifications were performed using WinMDI 2.9 software.

## Neutral comet assay

DSBs were measured in VH10-TERT cells using the Comet Assay system (Trevigen) according to the manufacturer's instructions. Comet tail moments were scored using Comet Score software (TriTek).

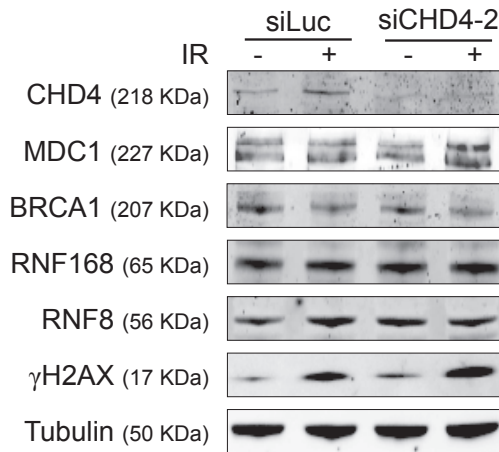
## Online supplemental material

Fig. S1 shows that depletion of CHD4 does not alter the expression level of DDR proteins after IR. Fig. S2 shows that MBD3-GFP, like GFP-CHD4, rapidly accumulates at sites of laser-induced DNA damage. Fig. S3 shows that CHD4 depletion reduces IR-induced  $\gamma$ H2AX ubiquitylation and that CHD4 ATPase activity is required for RNF168 IRIF formation. Online supplemental material is available at <http://jcb.rupress.org/content/190/5/741/suppl/DC1>

## Acknowledgements

We thank Jiri Lukas, Dan Durocher, Adrian Bird, Ody Sibon, Mauro Modesti and Jacob Aten for providing reagents. We acknowledge Ron Romeijn for constructing pEGFP-C1-MTA2, Antoine de Morrée for technical advice, Karien Wiesmeijer, Annelies van der Laan, Roeland Dirks, Przemek Krawczyk and Jacob Aten for assistance with the micro-laser irradiation and Jiri Lukas for sharing results prior to publication. This work was supported by a VIDI grant from the Netherlands Organization for Scientific Research (NWO).

## SUPPLEMENTARY FIGURES



**Figure S1. Depletion of CHD4 does not alter the expression level of DDR proteins after IR.** U2OS cells were transfected with the indicated siRNA and exposed to 3 Gy of IR. 1 h later WCE were prepared and protein levels were monitored by western blot analysis.

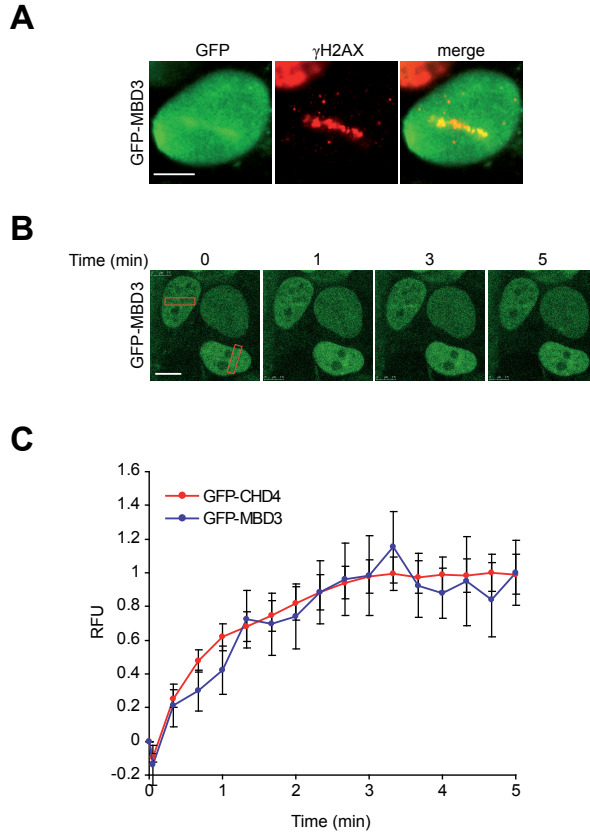


**Figure S2. MBD3 rapidly accumulates at sites of DNA damage.** (A) GFP-MBD3 accumulates in DSB-containing regions marked by  $\gamma$ H2AX. U2OS cells transiently expressing GFP-MBD3 were subjected to laser micro-irradiation. 15 min later cells were immunostained for  $\gamma$ H2AX. (B) GFP-MBD3, like GFP-CHD4, rapidly accumulates in DSB-containing regions. U2OS cells transiently expressing GFP-MBD3 or GFP-CHD4 were micro-irradiated as in A and subjected to real-time recording of protein assembly at the damaged area. (C) Quantitative representation of the results in B. RFU are plotted on a time scale. Graphs represent the mean  $\pm$  s.e.m. of at least 10 individual cells from at least 2 independent experiments. Scale bars, 10  $\mu$ m.

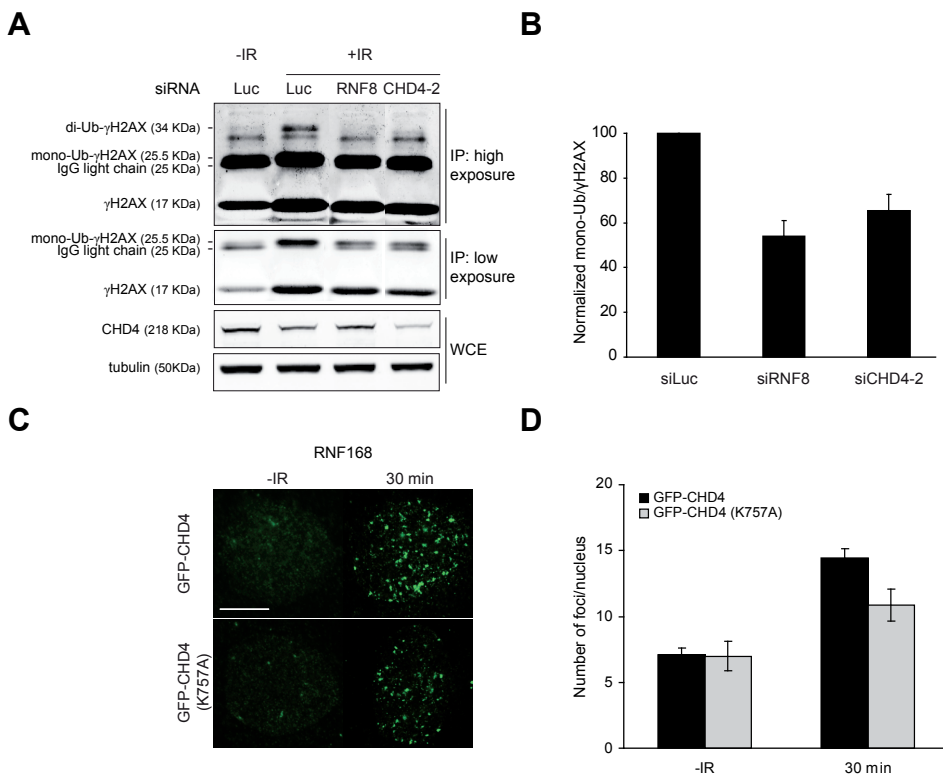


**Figure S3. CHD4 affects the IR-induced RNF8/RNF168 ubiquitin response.** (A) CHD4 depletion impairs IR-induced  $\gamma$ H2AX ubiquitylation. Cells were transfected with the indicated siRNAs and exposed to 10 Gy of IR. 1 h later WCE and chromatin-enriched extracts (CEE) were prepared. CEE were subjected to immunoprecipitation (IP) with  $\gamma$ H2AX antibody. Western blot analysis of IP with  $\gamma$ H2AX antibody, and WCE with CHD4 and tubulin antibodies is shown. (B) Graphical representation of relative  $\gamma$ H2AX ubiquitylation levels determined using cells from A. Ratios of  $\gamma$ H2AX mono-ubiquitylation and  $\gamma$ H2AX were calculated and normalized to that of control cells, which was set to 1, respectively. The mean  $\pm$  s.e.m. of 3 experiments is shown. (C) CHD4 ATPase activity is required for RNF168 IRIF formation. Cells were transfected with pEGFP-C1-CHD4 or pEGFP-C1-CHD4(K757A), which expresses a dominant-negative, ATPase-dead form of CHD4, and 1 day later exposed to 1 Gy of IR. After 30 min cells were immunostained for RNF168 (D). Quantitative analysis of RNF168 IRIF formation. The average number of foci/nucleus  $\pm$  s.e.m. is presented. More than 100 nuclei from cells in C were scored per time point in 2 independent experiments. Scale bar, 10  $\mu$ m.



